Geochemistry Geophysics Geosystems G3
AN ELECTRONIC JOURNAL OF THE EARTH SCIENCES
Published by AGU and the Geochemical Society

Article
Volume 9, Number 11
6 November 2008
Q11T04, doi:10.1029/2008GC002070
ISSN: 1525-2027

Navigational infrastructure at the East Pacific Rise 9°50′N area following the 2005–2006 eruption: Seafloor benchmarks and near-bottom multibeam surveys

S. A. Soule
Geology and Geophysics, Woods Hole Oceanographic Institution, 286 Woods Hole Road, Woods Hole, Massachusetts 02543, USA (ssoule@whoi.edu)

V. L. Ferrini
Lamont Doherty Earth Observatory, Columbia University, 61 Route 9W, Palisades, New York 10964, USA

J. C. Kinsey
Applied Ocean Physics and Engineering, Woods Hole Oceanographic Institution, 286 Woods Hole Road, Woods Hole, Massachusetts 02543, USA

D. J. Fornari
Geology and Geophysics, Woods Hole Oceanographic Institution, 286 Woods Hole Road, Woods Hole, Massachusetts 02543, USA

C. Sellers
Applied Ocean Physics and Engineering, Woods Hole Oceanographic Institution, 286 Woods Hole Road, Woods Hole, Massachusetts 02543, USA

S. M. White
Department of Geological Sciences, University of South Carolina, Columbia, South Carolina 29208, USA

K. Von Damm
Department of Earth Science, University of New Hampshire, Durham, New Hampshire 03824, USA

Deceased 15 August 2008

S. M. Carbotte
Lamont Doherty Earth Observatory, Columbia University, 61 Route 9W, Palisades, New York 10964, USA

[1] Four seafloor benchmarks were deployed with ROV *Jason2* at frequently visited areas along the northern East Pacific Rise (NEPR) ridge crest near 9°50′N, within the Ridge2000 EPR integrated study site (ISS) bull's eye. When used in concert with established deep-ocean acoustic positioning techniques, these benchmarks provide navigational infrastructure to facilitate the integration of near-bottom data at this site by allowing efficient and quantitative coregistration of data and observations collected on multiple dives and over multiple cruises. High-resolution, near-bottom multibeam bathymetric surveys also were conducted along and across the ridge crest to provide a morphological and geological context for the benchmark areas. We describe the navigation and data processing techniques used to constrain the benchmark positions and outline operational details to effectively use benchmarks at this and other deep-ocean sites where multidisciplinary time series studies are conducted. The well-constrained positions of the

benchmarks provide a consistent geospatial framework that can be used to limit navigational uncertainties during seafloor sampling and mapping programs and enable accurate spatial coregistration and integration of observations. These data are important to test a range of multidisciplinary hypotheses that seek to link geological, chemical, and biological processes associated with crustal accretion and energy transfer from the mantle to the hydrosphere at mid-ocean ridges.

Components: 6629 words, 7 figures, 3 tables.

Keywords: mid-ocean ridge; bathymetry; navigation; acoustic; hydrothermal vent.

Index Terms: 3080 Marine Geology and Geophysics: Submergence instruments: ROV, AUV, submersibles; 3045 Marine Geology and Geophysics: Seafloor morphology, geology, and geophysics.

Received 23 April 2008; **Revised** 29 August 2008; **Accepted** 11 September 2008; **Published** 6 November 2008.

Soule, S. A., V. L. Ferrini, J. C. Kinsey, D. J. Fornari, C. Sellers, S. M. White, K. Von Damm, and S. M. Carbotte (2008), Navigational infrastructure at the East Pacific Rise 9°50′N area following the 2005–2006 eruption: Seafloor benchmarks and near-bottom multibeam surveys, *Geochem. Geophys. Geosyst.*, *9*, Q11T04, doi:10.1029/2008GC002070.

Theme: Recent Volcanic Eruptions, Properties, and Behavior of the Fast Spreading East Pacific Rise at 8°–11°N
Guest Editors: S. Carbotte, R. Haymon, and B. Seyfried

1. Introduction

[2] Over the past 25 years, regional-scale investigations of ridge-crest characteristics at sites such as the fast spreading northern East Pacific Rise (NEPR) have provided an important framework for understanding the structure and evolution of mid-ocean ridges (MORs) [e.g., *Macdonald et al.*, 1984, 1992; *Lonsdale*, 1983; *Fornari et al.*, 1984; *Crane*, 1985; *Edwards et al.*, 1991; *White et al.*, 2006]. With advances in deep submergence technology over the last decade, near-bottom studies of geological, biological, and hydrothermal features along the ridge crest have been effective at characterizing the interconnected fine-scale active processes operating at the plate boundary [e.g., *Haymon et al.*, 1993; *Shank et al.*, 1998; *Fornari et al.*, 1998, 2004; *Von Damm and Lilley*, 2004; *Tolstoy et al.*, 2008; *Lowell et al.*, 2008]. Successful integration of these diverse sets of multiscalar data requires well-constrained navigation to ensure precise spatial coregistration of interdisciplinary scientific observations collected over multiyear periods. For example, biologists studying vent fauna succession at hydrothermal sites need sufficient positional accuracy to relate their observations to changes in fluid chemistry measured by geochemists on multiyear cruises to the same site. As large-scale database efforts (e.g., www.marine-geo.org) [*Carbotte et al.*, 2004] have begun to compile seafloor data and observations, the need for precise navigational data has become increasingly important to ensure that ongoing studies can successfully and quantitatively build upon previous work.

[3] We report on the deployment of a set of physical benchmarks accompanied by localized high-resolution bathymetric surveys within the integrated study site (ISS) of the Ridge2000 program at 9°50′N on the NEPR (Figure 1). In concert with established deep-ocean acoustic navigational techniques, these benchmarks and bathymetric maps provide the navigational infrastructure to ensure adequate positional accuracy to support long-term and multidisciplinary time series observations. The benchmarks are easily identifiable physical markers within a known geologic context and can provide real-time guidance to frequently visited sites. The well-constrained seafloor positions of the benchmarks provide a geospatial baseline that can be used to constrain navigational uncertainties by locating seafloor sampling, observations, and mapping within a consistent navigational framework.

[4] The use of benchmarks for real-time guidance builds upon the success of the bio-geo transect [*Shank et al.*, 1998], a series of markers placed along the floor and margin of the axial summit trough (AST) that were used as navigational aids after the 1991–1992 eruptions at the NEPR [e.g., *Haymon et al.*, 1993; *Rubin et al.*, 1994; *Gregg et al.*, 1996] until their destruction during the 2005–2006 eruption [e.g., *Tolstoy et al.*, 2006; *Cowen et al.*, 2007; *Soule et al.*, 2007]. The dynamic nature of the AST floor, which has been modified by at

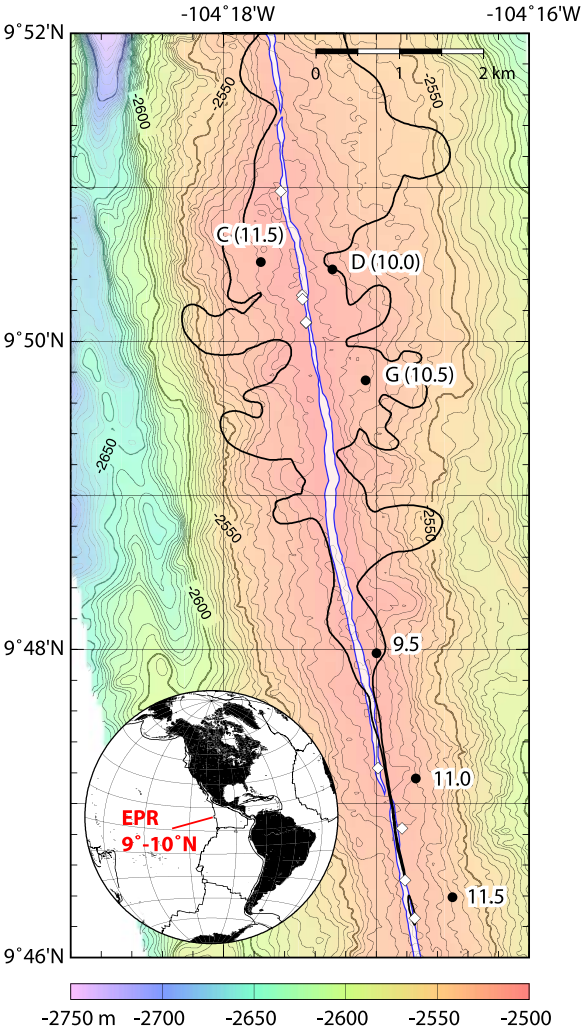

Figure 1. EM300 multibeam bathymetry [*White et al.*, 2006] of the northern East Pacific Rise (NEPR) crest where numerous deployed experiments and near bottom studies are facilitated by the Ridge2000 program. The black line shows areas covered by the recent volcanic eruption in 2005–2006. White diamonds mark high-temperature vents. A blue line shows the position of the axial summit trough. An array of six bottom-moored acoustic transponders (and transmit frequency) positioned along the ridge crest are shown by black dots (Table 1).

least two major eruptive events since 1991, as well as the collapse and expansion of hydrothermal vent structures over short timescales, prescribes the need for physical markers and guided our selection of deployment sites for the new benchmarks.

2. National Deep Submergence Facility Vehicle Navigation

[5] National Deep Submergence Facility (NDSF) vehicles (*Alvin*, *Jason2*, *Sentry*; www.whoi.edu/ndsf) are navigated through the integration of Doppler Velocity Log (DVL) sonars, pressure depth sensors, north-seeking fiber-optic gyroscopes, and long baseline (LBL) acoustic navigation systems [*Kinsey and Whitcomb*, 2004]. Errors on the order of submeter to tens of meters that commonly occur in DVL-based vehicle position estimates due to a variety of error sources (e.g., loss of DVL bottom-lock; cumulative drift) [*Kinsey et al.* 2006a], can be removed by postprocessing of DVL navigation data resulting in improved vehicle navigation accuracy [*Ferrini et al.*, 2005, 2007; *Kinsey and Whitcomb*, 2004]. Improvement in accuracy is variable within a dive and can be as large as 20 m.

[6] Geospatially referenced Doppler positions are obtained through integration with LBL acoustic navigation in which the vehicle position is computed from acoustic ranges within a network of moored transponders. When depth measurements are available, only two ranges are required to compute the XY position using triangulation. If additional ranges are available a least squares solution can be employed to improve the accuracy of the position estimate. LBL navigation provides position measurement at intervals of 10–30 s with a range-dependent precision of 0.2–20 m [*Hunt et al.*, 1974; *Milne*, 1983]. LBL navigation requires careful placement of transponders (e.g., transponders deployed in high-relief terrain may suffer from acoustic shadowing and/or possible reception of reflected acoustic pings) and accurate surveying of transponder positions [*Lerner et al.*, 1999; *Kinsey et al.* 2006a]. Errors in transponder positions may also arise from watch circle drift on the order of 1–10 m over 1–10 h timescales (with a tether length of 150 m) due to ocean currents.

3. Navigational Infrastructure at NEPR

[7] Six Benthos XT6001 acoustic transponders were permanently deployed at the NEPR in 2006 (AT15–06; Chief Scientist: Von Damm) and 2007 (AT15–27; Chief Scientist: Klein) to provide a consistent LBL acoustic network for interdisciplinary studies (Figure 1) and obviate the need to deploy, survey, and recover transponders. The transponders cover the area between 9°51′N (Bio-vent) and 9°46–47′N (A and L vents) where high- and low-temperature (high-T, low-T) hydrothermal vents and biological communities are being studied [e.g., *Shank et al.*, 1998; *Von Damm and Lilley*, 2004]. Each transponder is on a 152 m tether to minimize acoustic shadowing within the primary

Table 1. Transponder Locations at the 9°50′N East Pacific Rise Integrated Study Site Used for Long Baseline Position Estimates[a]

Transponder	X Position	Y Position	Depth	Latitude	Longitude
C	4113.0	78369.0	2343.0	9°50.514′N	104°17.755′W
D	4972.0	78283.0	2344.0	9°50.467′N	104°17.286′W
G	5369.0	76952.0	2354.0	9°49.745′N	104°17.069′W

[a] See Figure 1 for map location.

working area of the ISS. Operations reported here occurred near 9°50′N, within acoustic range of the three northernmost transponders listed in Table 1; the positions of all NEPR transponders are listed in the Ridge 2000 Data Portal (http://www.marine-geo.org/link/station_groups.php?feature_id=EPR&subset=current).

[8] A least squares estimate of transponder 3-D positions is computed from ~100 range measurements (between a ship-mounted transducer and the transponder on the seafloor) and the ship's GPS position. Thus, the quality of transponder position estimates depends in part on the precision of the ship's GPS system. The NEPR transponder surveys were all conducted from the R/V *Atlantis*, which is equipped with a Furuno GP-90 GPS system (nominal accuracy: 5 m). The precision (i.e., 1-sigma) of this GPS system, based on data obtained while the vessel was docked is ±2.29 m and ±2.44 m for X and Y, respectively. The RMS positioning error of each transponder survey (duration less than 1 h) is less than 0.5 m (Table 1).

4. Benchmark Deployments and Positions

[9] Four benchmarks were deployed outside of the AST along the NEPR during *Jason2* lowering 268 in April 2007. Although the seafloor mapped during benchmark surveys was clearly covered by new lava during the 2005–2006 eruption, the benchmarks should remain undisturbed if volcanic activity is limited to within the AST as was inferred for the 1991–1992 NEPR eruption [e.g., *Haymon et al.*, 1993; *Gregg et al.*, 1996]. The benchmarks were designed to provide accurate and unique identification in both horizontal and vertical incidence imaging (Figure 2). After deploying a benchmark and ballasting it with rocks, the ROV faced north and rested on the seafloor with the benchmark immediately in front of the retracted tool

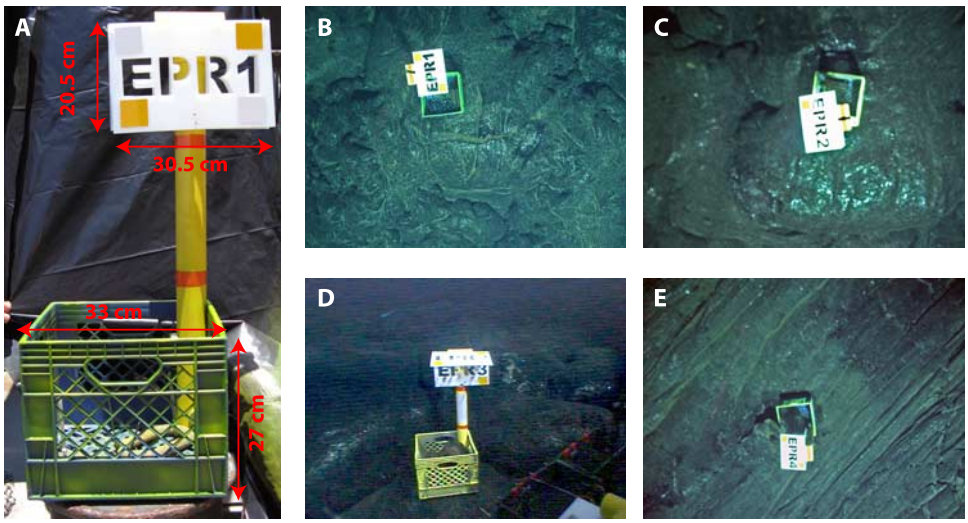

Figure 2. (a) Seafloor benchmarks used in this study were constructed from milk crates, in which rock ballast was placed upon deployment. Labels are cut out of a hinged polyvinyl nameplate (20.5 × 30.5 cm) attached to a stanchion. Cutouts help minimize biofouling of labels. The total height of each benchmark is ~1 m. The nameplate is made of two identical placards, the free portion of which is able to float, allowing the nameplates to be identified from above and from the side. (b–d) Digital photographs taken from *Jason2* of the four installed EPR integrated study site (ISS) benchmarks from above (benchmarks 1, 2, and 4) and obliquely (benchmark 3) illustrate the visibility of the benchmarks and the substrate on which they were placed.

Table 2. Computed Positions of the Benchmarks[a]

Benchmark	Solution Method	Number of LBL Cycles	Transponders	X Position Mean (2-sigma) (m)	Y Position Mean (2-sigma) (m)
1	least squares	88	C, D, G	4273.65 (2.69)	79220.65 (2.50)
1	**2 range**	**114**	**C, D**	**4274.14 (2.37)**	**79222.91 (0.92)**
1	2 range	138	C, G	4275.95 (1.23)	79222.64 (0.65)
1	2 range	85	D, G	4270.42 (7.69)	79219.86 (3.88)
2	**least squares**	**89**	**C, D, G**	**4623.60 (0.23)**	**78171.91 (0.25)**
2	2 range	89	C, D	4623.44 (0.22)	78168.73 (0.56)
2	2 range	89	C, G	4625.06 (0.41)	78172.93 (0.42)
2	2 range	89	D, G	4622.57 (0.29)	78171.41 (0.23)
3	**least squares**	**93**	**C, D, G**	**4643.82 (0.27)**	**77995.33 (0.30)**
3	2 range	96	C, D	4643.29 (0.25)	77990.71 (0.25)
3	2 range	96	C, G	4650.78 (0.81)	78001.44 (0.83)
3	2 range	96	D, G	4640.25 (0.27)	77994.16 (0.26)
4	**least squares**	**195**	**C, D, G**	**4732.06 (0.57)**	**77649.92 (0.28)**
4	2 range	195	C, D	4731.91 (0.58)	77647.55 (0.23)
4	2 range	195	C, G	N/A	N/A
4	2 range	196	D, G	4728.80 (0.90)	77648.73 (0.18)

[a] Bold positions represent the highest precision estimates. Here LBL is long baseline.

basket. LBL position measurements were collected once every 15 s for approximately 15 min.

[10] Benchmark positions were recomputed after the dive using ranges from the three transponders located in the vicinity (transponders C, D, and G; Table 2). Since the transponders and the vehicle were deeply submerged, acoustic refraction was considered negligible. Acoustic travel times from all three transponders enabled us to compute conventional two-transponder LBL solutions using each of the transponder pairs (CD, CG, and DG; Table 2) and a least squares solution using ranges from all three transponders [e.g., *Milne*, 1983; *Hunt et al.*, 1974]. At each benchmark, four position estimates were computed for each LBL cycle, and the mean of the estimates over the 15-min survey period was computed to determine the final position for each method. Mean positions are listed in Table 2, with the standard deviations of each technique's estimate listed in parentheses.

[11] Using the number of LBL cycles and the standard deviations as criteria, we identify the most accurate mean position estimate for each benchmark (shown in bold in Table 2). In cases where the two-range solutions and the least squares possessed comparable LBL cycles and standard deviations (e.g., the C–D, D–G, and least squares solutions for benchmark 3), the least squares solution was preferred. The close proximity of benchmark 4 to the baseline between transponders C and G precluded obtaining estimates using the CG two-transponder solution.

[12] To illustrate our methodology, consider the estimation of the XY position of benchmark 2 (Figure 3). During the 15-min survey between 2305 and 2320 on 20 April 2007, all 89 LBL ping cycles contained returns from all three transponders. Figure 3a shows the X and Y position estimates computed by each technique for benchmark 2 versus time. The right plot shows the distribution of the position estimates for each of the techniques. The least squares solution and the DG transponder pair solution possess the lowest standard deviations. The norm of the standard deviations for the least squares solution is 0.34 m (compared to 0.37 m for the DG transponder pair solution), and thus the least squares solution was used as the position of benchmark 2 (bold line in Figure 3). Subsequent surveys of benchmarks 2 and 3 carried out ~12 h after the first survey are all within 0.2 m of the calculated positions reported in Table 2.

[13] Positions of several hydrothermal vent sites within the study area that are frequently visited: Bio9, P, Ty, and Io, were also evaluated using 2 and 3 transponder solutions. The vehicle sat on the seafloor at the vent sites for periods of 5–20 min. As these surveys were conducted during sampling operations, vehicle heading was prescribed by the position of active vents. Table 3 shows the most accurate vent positions determined during the surveys; each position has a precision of ~0.5 m.

5. Multibeam Bathymetry Surveys

[14] High-resolution bathymetry data were collected during J2–268 with a 200 kHz Simrad SM2000 multibeam sonar system mounted on *Jason2*. Sur-

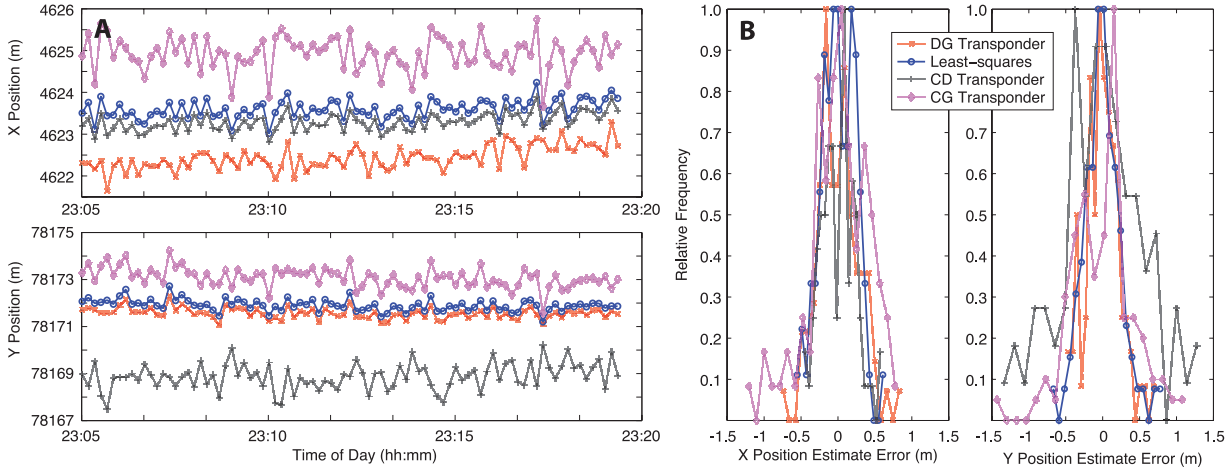

Figure 3. (a) Plots of the X and Y positions of benchmark 2 based on long baseline (LBL) acoustic navigation data versus time of day (see Table 2 for details) during one of the benchmark surveys conducted during *Jason2* Dive 268 on 20 April 2007. (b) Each of the four solution techniques show a Gaussian distribution of X and Y position errors (position minus mean position over the 15 min time interval) about a mean of ~0. In this case, the least squares method was selected as the best result (bold lines in Figure 3b) as it has the least variance over the duration of the survey. The position estimates listed for benchmark 2 in Table 3 are the mean of the calculated position estimates (Figure 3a); the standard deviations (1-sigma) correspond to the error histograms (Figure 3b).

veys were conducted across the AST at each benchmark site and along the AST between all benchmarks (Figure 4). The portions of the AST imaged in these surveys hosted the eruptive vents of both the 1991–1992 and 2005–2006 eruptions and contain hydrothermal vents and vent structures that remained active through the most recent volcanic cycle. Over the past 15 years, these sites have been visited frequently and are likely to be visited in the future. These surveys represent snapshots of the morphologic character and arrangement of hydrothermal, tectonic, and volcanic features of the axial region that can serve as a baseline for assessing small-scale changes resulting from fault slip, lava deposition, mass wasting, and hydrothermal vent construction/destruction.

[15] Multibeam data were collected using a line spacing of ~25 m, and vehicle altitude did not exceed 30 m. Surveys were conducted in set-point depth control, i.e., vehicle depth was constant throughout and the seafloor was allowed to rise and fall beneath it (Figure 4b). Data were processed using the standard NDSF techniques for postprocessing navigation [*Ferrini et al.*, 2005, 2007; *Kinsey et al.*, 2006b] and bathymetric data [*Ferrini et al.*, 2007, and references therein]. Spurious LBL position data were manually removed and the DVL velocity data reintegrated to obtain improved vehicle position estimates. Edited LBL data and reintegrated DVL data were merged using a complementary filter, which low-pass filters less precise LBL positions and high-pass filters the more precise DVL data to create a more accurate vehicle navigational track [*Whitcomb et al.*, 1999; *Ferrini et al.*, 2008]. The resulting navigation data were merged with sonar and attitude data to generate bathymetric soundings. Bathymetric data were quality-controlled using the Fledermaus® 3-D editor. Bathymetric data points and 1-m grids are available through the Ridge 2000 Data Portal (http://www.marine-geo.org/link/entry.php?id=AT15-17). We present below a basic description of the seafloor morphological and geological context at each benchmark site, the latter constructed from near-bottom observations (video and still imagery) col-

Table 3. Long Baseline Three-Transponder Solution Surveyed Positions of High-Temperature Vent Sites at the 9°50′N Area on the Northern East Pacific Rise Axis

Vent	X Position (m)	Y Position (m)	Depth (m)	Latitude	Longitude
Bio9	4609.49	77992.78	2509	9°50.313′N	104°17.484′W
P	4623.29	78171.91	2501	9°50.279′N	104°17.473′W
Ty	4643.83	77995.36	2501	9°50.118′N	104°17.440′W
lo	4732.06	77649.91	2503	9°50.112′N	104°17.426′W

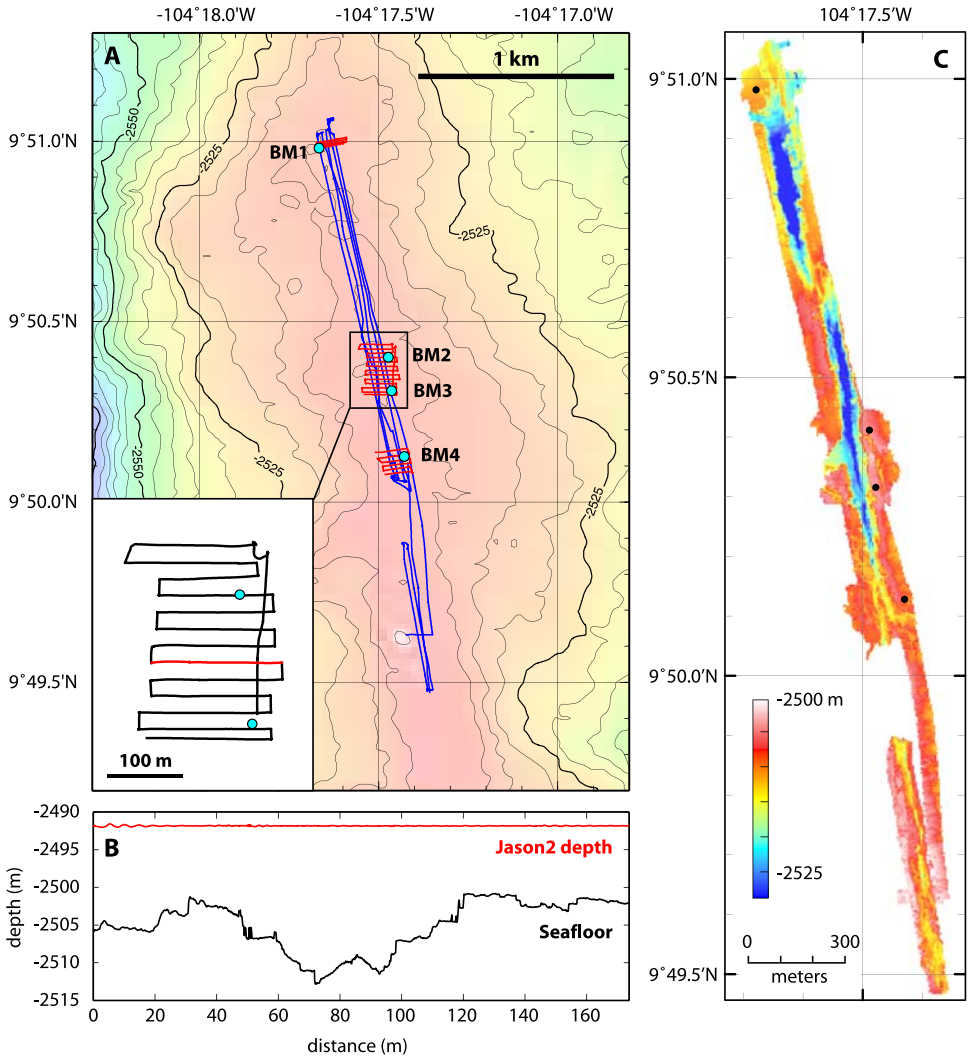

Figure 4. (a) Tracklines for near-bottom multibeam bathymetry surveys along axis (blue) and at the benchmarks (red) shown over the EM300 regional bathymetry [*White et al.*, 2006]. Benchmark positions are shown as cyan dots. An approximate line spacing of 25 m was maintained during benchmark surveys (see map inset). (b) Surveys were conducted in a "constant depth" mode, where vehicle depth was maintained and the seafloor allowed to rise and fall beneath the vehicle (shown for the red track line in Figure 4a inset). (a) SM2000 multibeam bathymetry (gridded at 5-m) for the along-axis survey between 9°49.5′N and 9°51′N, covering the area between the benchmarks (black dots).

lected on this and several other cruises to the sites [e.g., *Cowen et al.*, 2007; *Soule et al.*, 2007].

5.1. Benchmark 1 Area

[16] Benchmark 1 was placed on a platform of lobate lava west of the AST near BioVent, a high-temperature vent that has been monitored and sampled since it became active after the 1991 eruption [*Von Damm*, 2004; *Scheirer et al.*, 2006] (Figure 5). The benchmark is 50 m west of the western AST wall, and 70 m north-northwest of BioVent (bearing: 284°). Several local collapse features [e.g., *Engels et al.*, 2003] are evident between the benchmark location and the AST wall. The AST at this location contains several parallel fissures (Figure 5) within a ~75 m wide trough, the eastern margin of which is poorly defined. The AST floor is covered with broken (i.e., collapsed) lava crusts with patches of intact lobate and sheet lava flows and scattered lava pillars. We interpret pervasive collapse east of the AST rim based on the slightly deeper and irregular nature of the seafloor as displayed in the near-bottom multibeam data relative to the uppermost lobate platform. An east-west oriented depression that is imaged in the far east of the survey contains lineated sheet flows that are common in lava channels [*Soule et al.*, 2005; *Garry et al.*, 2006].

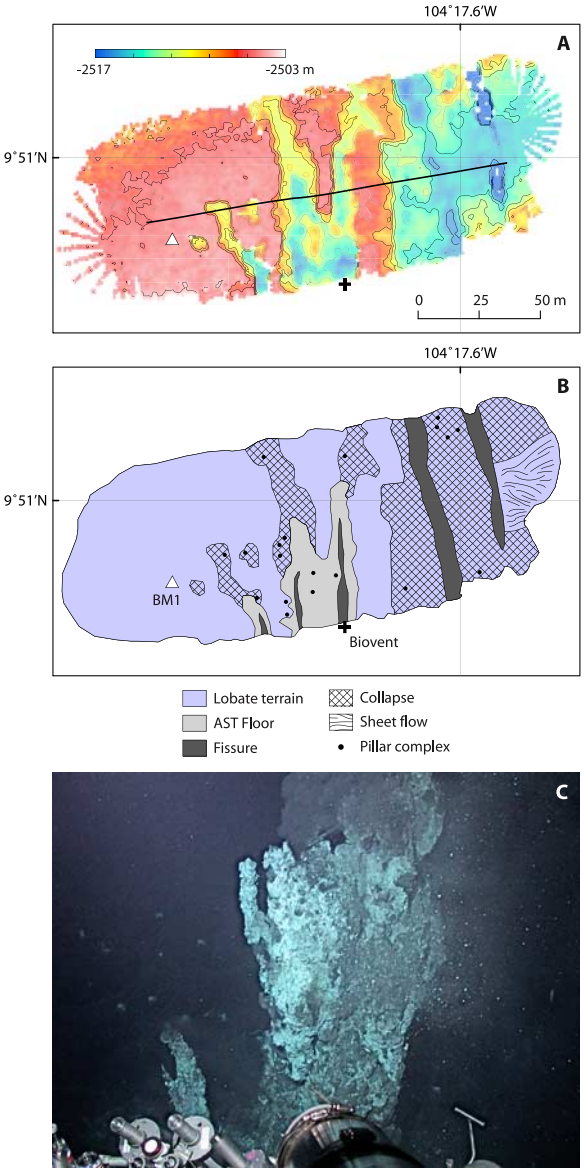

Figure 5. Benchmark 1 near-bottom SM2000 multibeam bathymetry survey and interpretation. (a) Bathymetry data are gridded at 1 m and shown with 1 m contours. The white triangle shows the position of benchmark 1 (Table 2) and the black cross shows the position of Biovent (Table 3). The black line marks the location of a photo transect conducted during *Jason2–268*. (b) Interpretation based on near-bottom imagery and bathymetry shows numerous fissures and collapse within the AST and pervasive collapse east of the AST rim. A lava channel is present at the east edge of the survey. (c) Photo of Biovent taken from Alvin on dive 4374 in 2007.

5.2. Benchmark 2–3 Area

[17] Benchmarks 2 and 3 were placed on lobate lava crust at the eastern margin of the AST near three vent sites (Tica, Bio9, and P) that have been studied extensively over the past 10 years [e.g., *Shank et al.*, 1998; *Von Damm and Lilley*, 2004; *Scheirer et al.*, 2006] (Figure 6). Benchmark 2 is located ~30 m east of the currently low-T diffuse venting site Tica (bearing: 80°); benchmark 3 is located near two high-T hydrothermal vents, ~20 m east of Bio9 (bearing: 80°) and ~50 m north-northeast of P (bearing: 12°). Although the seafloor in the benchmark 2 and 3 survey area is covered with lava from the 2005–2006 eruption, the sites of active venting at Bio9 and P-vent were not significantly altered.

[18] The new bathymetry reveals a well-developed AST ~50 m wide and ~12 m deep. The AST walls are steep, and in many places the margins have overhanging lava crusts supported by lava pillars [e.g., *Chadwick*, 2003]. The terrain at the crest of the AST is composed of lobate lava flows and contains areas of localized collapse (0.5 to ~1.0 m deep). A bench, located ~2 m below the primary ridge crest surface is present along the western wall of the AST. In the southern part of the survey area it comprises a narrow bench along the AST wall. In the north, a lava channel is present across a more extensive secondary platform (Figure 6). The AST floor in this area is a complex terrain of broken lava crusts along with lobate and sheet lava flows. The 2–5 m-deep troughs that extend west of the AST and connect to the AST floor represent older lava channels and were present before the 2005–2006 eruption [e.g., *Soule et al.*, 2005]. They are currently floored by lobate lava emplaced during the 2005–2006 eruption. A primary eruptive fissure, less than 15 m wide and 2–4 m deep, is evident at the center of the AST. The fissure tapers and reemerges toward the southern part of the survey area [*Ferrini et al.*, 2007], illustrating the fine-scale segmentation visible in the new high-resolution bathymetry data.

[19] Two high-T hydrothermal vent sites (Bio9, P) are resolved in the bathymetry, appearing as mounds 5–10 m across and 2–5 m high, morphologically similar to nearby lava pillar complexes. The vent sites occur within the AST floor and are composed of multiple narrow sulfide chimneys, only 1 or 2 of which may be active at any given time. The individual chimneys are 2–8 m high and commonly only a meter in diameter. The vent areas contain sulfide debris from fallen chimneys, but in many places the basalt substrate can also be seen (Figure 6c). The Bio9 vent site is ~10 m inside the eastern AST wall; P-vent is adjacent to the eastern AST wall. Diffuse vent sites in each area are not

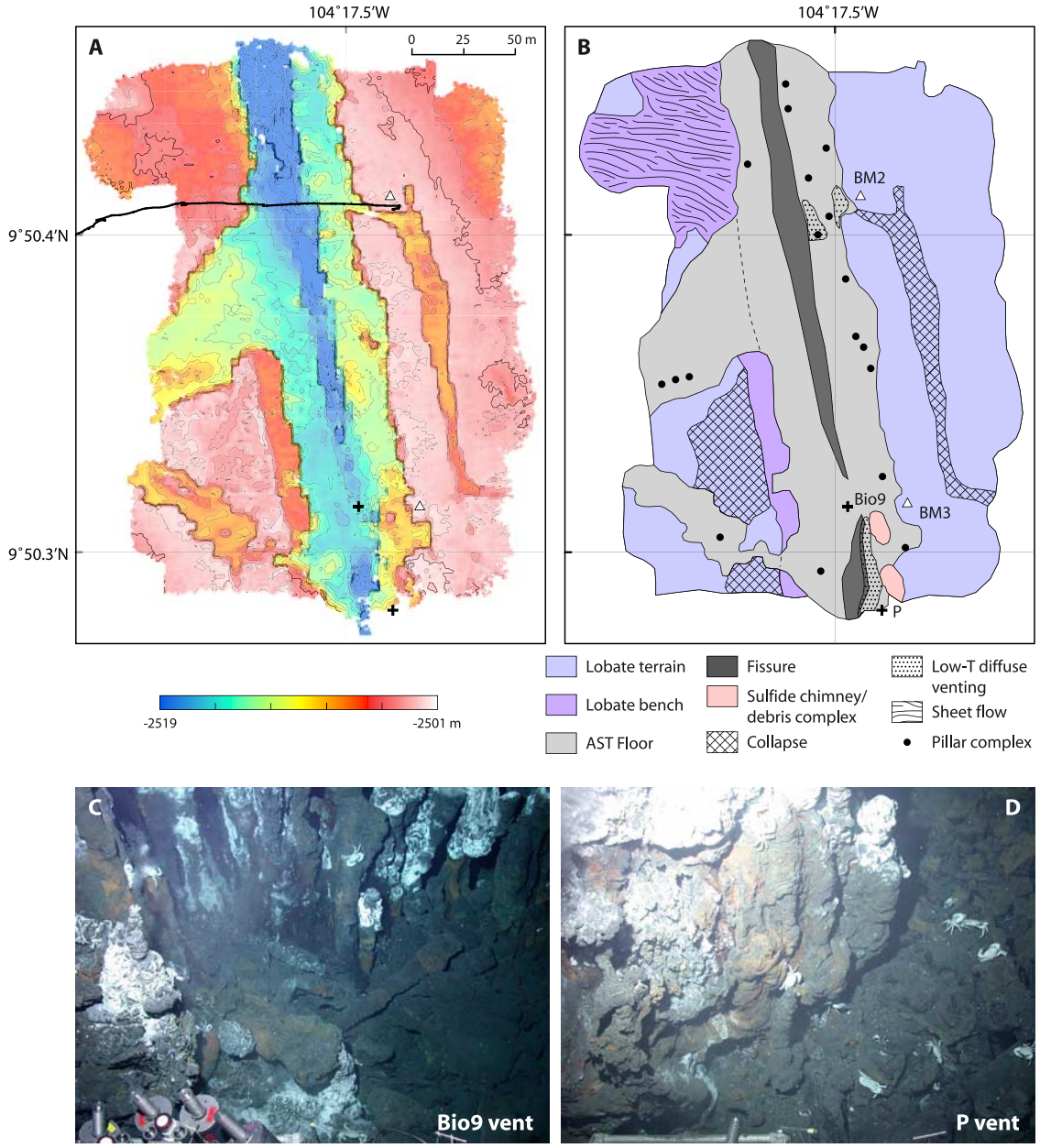

Figure 6. Benchmark 2–3 near-bottom SM2000 multibeam bathymetry survey and interpretation. (a) Bathymetry data are gridded at 1 m and shown with 1 m contours. The white triangles show position of benchmark 2 (north) and 3 (south) (Table 2) and black crosses show the position of Bio9 (north) and P (south) vents (Table 3). The black line marks the location of a photo transect conducted during *Jason2–268*. (b) Interpretation of bathymetry data indicates a well-defined AST ~40–60 m wide that contains the vent areas. Vent sites comprise numerous small sulfide chimneys covering ~5 m × 10 m areas that are elongate in the north-south direction along the trace of the primary fissure in the AST floor. Alvin photographs collected on Dive 4381 in 2007 of (c) Bio9 and (d) P vent show the character of the sulfide chimneys.

expressed in the bathymetry data, although are commonly located at breaks in slope, such as at the edge of the AST or fissures within the AST (Figure 6d). The location of the vent sites, as determined solely from LBL transponder ranges (see section 5), are offset from the bathymetric expression of the vents by ~10 m. This navigational discrepancy is not unexpected as navigation for the bathymetric survey, as produced onboard, reflects merged LBL and DVL positional data. Refinement of the positional data is the subject of a separate study.

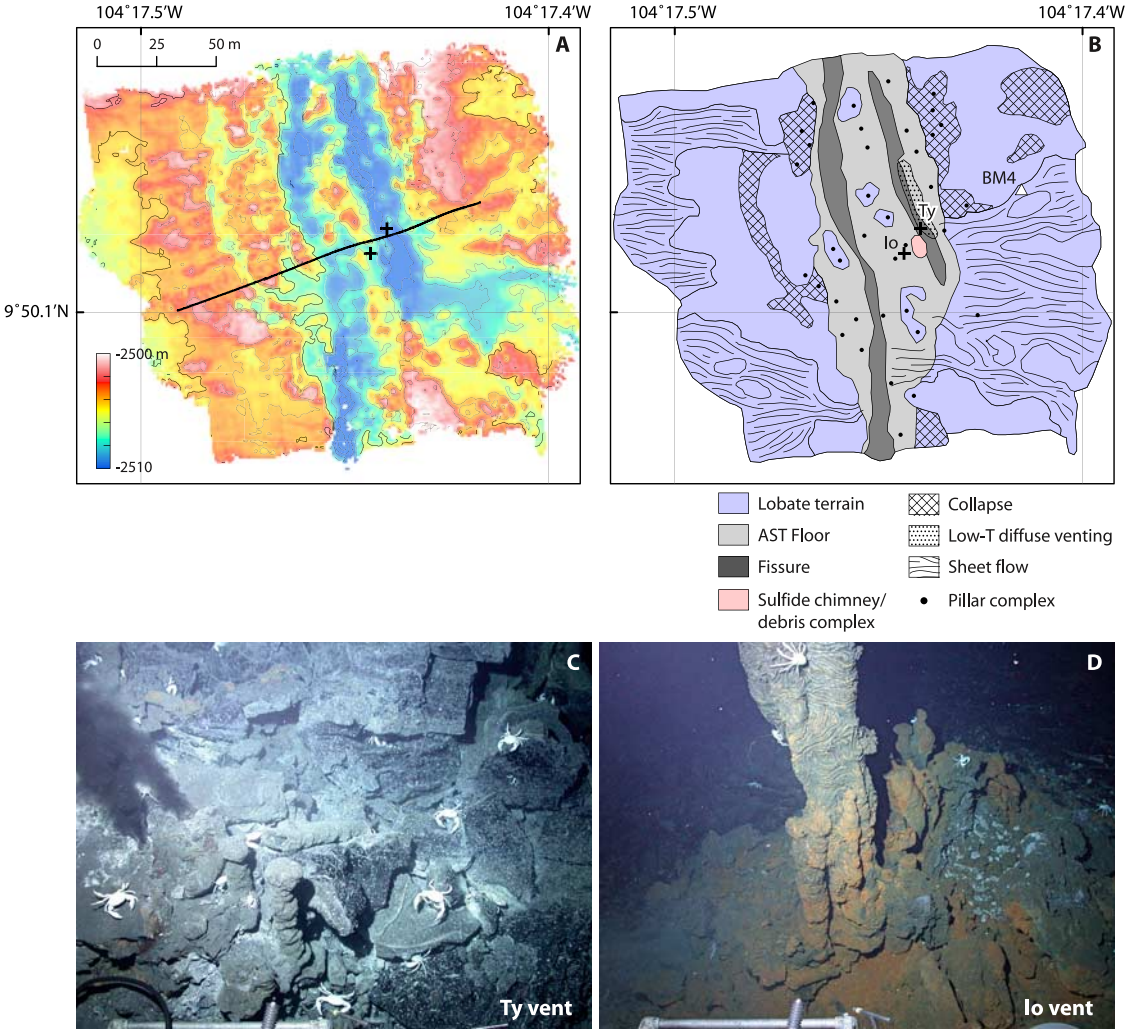

Figure 7. Benchmark 4 near-bottom SM2000 multibeam bathymetry survey and interpretation. (a) Bathymetry data are gridded at 1 m and shown with 1 m contours. The white triangle shows the position of benchmark 4 (Table 2) and black crosses show the position of Ty (east) and Io (west) vent sites (Table 3). (b) Interpretation of bathymetry indicates the AST has poorly defined walls and contains numerous lava pillars supporting remnant lava crusts created when the trough was filled with lava. Sheet flows emanate from the trough to the east and west, in places lacking a direct connection to the AST. Io vent site is characterized by a ~2 m × 5 m mound that is resolved by the detailed bathymetry and is elongate in the north-south direction. Alvin photographs taken on Dive 4381 in 2007 show (c) the small chimneys of the Ty site (note smoke at left edge of photograph) and (d) the larger, now inactive sulfide chimneys of the Io vent site.

5.3. Benchmark 4 Area

[20] Benchmark 4 was placed outside the AST, east of the Ty and Io vent sites, where biological experiments have been deployed [*Shank et al.*, 2006]. Benchmark 4 is ~50 m east-northeast of Io (bearing: 65°) and ~15 m northeast of Ty (bearing: 75°). The AST in this area is 40–60 m wide and 3–5 m deep and is less well defined than in the benchmark 2–3 area (Figure 7). In the northern part of the survey it is characterized by two parallel troughs, each containing a fissure, separated by a ridge of lobate lava crust remnants partially supported by lava pillars. The walls of the AST are extensively collapsed, leaving remnants of a volcanic carapace or platform. The platform is dominantly lobate lava, but this area is also characterized by abundant lineated sheet flows that drain the AST both to the west and east. The sheet flows mark the location of drained lava channels, the floors of which are 1–2 m lower than the lobate platform. Many of the lava channels are separated from the AST, where they were likely sourced, by lobate lava indicating either that late stage lobate

lava covered the proximal portions of the channels or that the channels were fed from underneath the lobate crust.

[21] The Io hydrothermal vent site is imaged in the bathymetry as a 5–10 m wide, 2–3 m high mound. The vent complex, which is extinct as of December 2007, was active at the time of our survey. It is comprised of a collection of narrow (<1 m diameter) sulfide chimneys with sulfide debris at their base (Figure 7c). The high-T vent Ty is located within a broad area of diffuse venting along the edge of the eastern fissure and is comprised of small (<1 m high) sulfide chimneys that are not resolved in the bathymetry data (Figure 7d).

6. Summary

[22] During a 3-day *Jason2* ROV dive, we placed four benchmarks along the NEPR ridge crest to serve as navigational controls to aid subsequent research programs conducting integrated time series measurements. We also conducted near-bottom multibeam bathymetry surveys in the vicinity of each benchmark and between benchmarks to provide geological context with respect to fine-scale volcanic, tectonic, and hydrothermal features on the ridge crest. The bathymetry data serve as a baseline for resolving future change in this portion of the ridge crest at spatial scales (<1 m vertically and <10 m^2 areally) relevant to active geological and hydrothermal processes.

[23] The benchmarks identify physical locations on the seafloor with known geographic positions and provide the infrastructure within which vehicle navigation can be better constrained. To effectively use benchmarks during seafloor operations, it is recommended that the submersible or ROV sit on the seafloor at the benchmark with a heading of 0° (see section 4). Remaining stationary at the benchmark site for ~15 min will provide sufficient data to compute the vehicle position and establish the quality of the navigation and quantify offsets between dives. At the conclusion of 15 min of navigation data collection, the benchmark position (Table 2) should be entered into the navigational software to reference the vehicle position within the established geospatial framework. When possible, revisiting the benchmark at the conclusion of on-bottom operations will provide the data necessary to quantify navigational offsets within each dive.

[24] Owing to the complexities of underwater vehicle navigation, spatial coregistration of time series observations can be challenging. The placement of benchmarks along the NEPR crest near frequently visited hydrothermal vent sites is intended to provide navigational infrastructure that can be utilized by the broad community of researchers actively studying the site. Utilizing benchmarks during multiple field programs will provide the data necessary to quantitatively coregister seafloor observations at a range of spatial and temporal scales.

Acknowledgments

[25] We thank the *Jason2* operations group of the NDSF and the officers and crew of R/V *Atlantis* for their excellent support during the survey and recovery operations on AT15–17 in general and specifically for Dive J2–268. E. Klein, chief scientist of AT15–17 graciously made available additional survey time, which allowed us to extend the along-axis SM2000 data collection. Program managers at the National Science Foundation, Ridge2000 Program Office, and shore-based support personnel at WHOI Marine Operations and NDSF were instrumental in funding and organizing the logistics for this EPR ISS survey. We are grateful to them for the opportunity to collect these data that will benefit both the Ridge2000 program and the EPR ISS community of researchers. We thank L. Mayer for a helpful review of the manuscript. Finally, we note with sadness the passing of one of our coauthors and colleagues, Karen Von Damm, and dedicate this paper to her in memory of her significant contributions to mid-ocean ridge science and the study of NEPR hydrothermal systems.

References

Carbotte, S. M., et al. (2004), New integrated data management system for Ridge2000 and MARGINS research, *Eos Trans. AGU*, *85*(51), 553, doi:10.1029/2004EO510002.

Chadwick, W. W. (2003), Quantitative constraints on the growth of submarine lava pillars from a monitoring instrument that was caught in a lava flow, *J. Geophys. Res.*, *108*(B11), 2534, doi:10.1029/2003JB002422.

Cowen, J. P., et al. (2007), Volcanic Eruptions at the East Pacific Rise near 9°50′N, *Eos Trans. AGU*, *88*(7), 81–83, doi:10.1029/2007EO070001.

Crane, K. (1985), The spacing of rift axis highs: Dependence upon diapiric processes in the underlying asthenosphere?, *Earth Planet. Sci. Lett.*, *72*, 405–414, doi:10.1016/0012-821X(85)90061-5.

Edwards, M. H., D. J. Fornari, A. Malinverno, W. B. F. Ryan, and J. Madsen (1991), The regional tectonic fabric of the East Pacific Rise from 12°50′N to 15°10′N, *J. Geophys. Res.*, *96*(B5), 7995–8018.

Engels, J. L., M. H. Edwards, D. J. Fornari, M. R. Perfit, and J. R. Cann (2003), A new model for submarine volcanic collapse, *Geochem. Geophys. Geosyst.*, *4*(9), 1077, doi:10.1029/2002GC000483.

Ferrini, V. L., D. Fornari, T. Shank, D. Kelley, M. K. Tivey, S. M. Carbotte, D. Glickson, C. Roman, and A. Sterling (2005), High-resolution sonar surveying at the R2K Integrated Study Sites: Techniques and strategies for improved

micro-bathymetric mapping, paper presented at Ridge 2000 Community Progress and Planning Workshop, Natl. Sci. Found., Vancouver, British Columbia, Canada.

Ferrini, V. L., D. J. Fornari, T. M. Shank, J. C. Kinsey, M. A. Tivey, S. A. Soule, S. M. Carbotte, L. L. Whitcomb, D. Yoerger, and J. Howland (2007), Submeter bathymetric mapping of volcanic and hydrothermal features on the East Pacific Rise crest at 9°50′N, *Geochem. Geophys. Geosyst.*, *8*, Q01006, doi:10.1029/2006GC001333.

Ferrini, V. L., M. K. Tivey, S. M. Carbotte, F. Martinez, and C. Roman (2008), Variable morphologic expression of volcanic, tectonic, and hydrothermal processes at six hydrothermal vent fields in the Lau back-arc basin, *Geochem. Geophys. Geosyst.*, *9*, Q07022, doi:10.1029/2008GC002047.

Fornari, D. J., W. B. F. Ryan, and P. J. Fox (1984), The evolution of craters and calderas on young seamounts: Insights from Sea Marc I and SeaBeam sonar surveys of a small seamount group near the axis of the East Pacific Rise at ~10°N, *J. Geophys. Res.*, *89*, 11,069–11,084, doi:10.1029/JB089iB13p11069.

Fornari, D. J., M. H. Edwards, R. M. Haymon, M. R. Perfit, and T. K. P. Gregg (1998), Axial summit trough of the East Pacific Rise 9°–10°N: Geological characteristics and evolution of the axial zone on fast spreading mid-ocean ridges, *J. Geophys. Res.*, *103*, 9827–9855, doi:10.1029/98JB00028.

Fornari, D. J., et al. (2004), Submarine lava flow emplacement at the East Pacific Rise 9°50′N: Implications for uppermost ocean crust stratigraphy and hydrothermal fluid circulation, in *Mid-Ocean Ridges: Hydrothermal Interactions Between the Lithosphere and Oceans*, *Geophys. Monogr. Ser.*, vol. 148, edited by C. R. German, J. Lin, and L. M. Parson, pp. 187–218, AGU, Washington, D.C.

Garry, W. B., T. K. P. Gregg, S. A. Soule, and D. J. Fornari (2006), Formation of submarine lava channel textures: Insights from laboratory simulations, *J. Geophys. Res.*, *111*, B03104, doi:10.1029/2005JB003796.

Gregg, T. K. P., D. J. Fornari, M. R. Perfit, R. M. Haymon, and J. H. Fink (1996), Rapid emplacement of a mid-ocean ridge lava flow on the East Pacific Rise at 9°46′–51′N, *Earth Planet. Sci. Lett.*, *144*, E1–E7, doi:10.1016/S0012-821X(96)00179-33.

Haymon, R. M., et al. (1993), Volcanic eruption of the mid-ocean ridge along the East Pacific Rise crest at 9°45–52′N: Direct submersible observations of seafloor phenomena associated with an eruption event in April, 1991, *Earth Planet. Sci. Lett.*, *119*, 85–101, doi:10.1016/0012-821X(93)90008-W.

Hunt, M. M., W. M. Marquet, D. A. Moller, K. R. Peal, W. K. Smith, and R. C. Spindell (1974), An acoustic navigation system, 70 pp., Woods Hole Oceanogr. Inst., Woods Hole, Mass.

Kinsey, J. C., and L. L. Whitcomb (2004), Preliminary field experience with the DVLNAV integrated navigation system for oceanographic submersibles, *Control Eng. Pract.*, *12*, 1541–1549, doi:10.1016/j.conengprac.2003.12.010.

Kinsey, J. C., R. M. Eustice, and L. L. Whitcomb (2006a), A survey of underwater vehicle navigation: Recent advances and new challenges, paper presented at Conference on Maneuvering and Control of Marine Craft, Int. Fed. of Autom. Control, Lisbon, Portugal.

Kinsey, J. C., L. L. Whitcomb, D. R. Yoerger, J. C. Howland, V. L. Ferrini, and O. Hegrenes (2006b), New navigation post-processing tools for oceanographic submersibles, *Eos Trans. AGU*, *87*(52), Fall Meet. Suppl., Abstract OS33A–1678.

Lerner, S., D. Yoerger, and T. Crook (1999), Navigation for the Derbyshire Phase 2 survey, 29 pp., Woods Hole Oceanogr. Inst., Woods Hole, Mass.

Lonsdale, P. (1983), Overlapping rift zone at the 5.5°S offset of the East Pacific Rise, *J. Geophys. Res.*, *88*, 9393–9406, doi:10.1029/JB088iB11p09393.

Lowell, R. P., , M. R. Perfit, J. Seewald, and A. Metaxas (Eds.) (2008), *Magma to Microbe: Modeling Hydrothermal Processes at Oceanic Spreading Centers*, *Geophys. Monogr. Ser.*, vol. 178, 300 pp., AGU, Washington, D.C.

Macdonald, K., J.-C. Sempere, and P. J. Fox (1984), East Pacific Rise from Siqueiros to Orozco fracture zones; along-strike continuity of axial neovolcanic zone and structure and evolution of overlapping spreading centers, *J. Geophys. Res.*, *89*, 6049–6069, doi:10.1029/JB089iB07p06049.

Macdonald, K. C., et al. (1992), The East Pacific Rise and its flanks 8–18°: History of segmentation, propagation and spreading direction based on SeaMARC II and SeaBeam studies, *Mar. Geophys. Res.*, *14*, 299–344, doi:10.1007/BF01203621.

Milne, P. H. (1983), *Underwater Acoustic Positioning Systems*, Gulf, Houston, Tex.

Rubin, K. H., J. D. Macdougall, and M. R. Perfit (1994), ^{210}Po-^{210}Pb dating of recent volcanic eruptions on the sea floor, *Nature*, *368*, 841–844, doi:10.1038/368841a0.

Scheirer, D. S., T. M. Shank, and D. J. Fornari (2006), Temperature variations at diffuse and focused flow hydrothermal vent sites along the northern East Pacific Rise, *Geochem. Geophys. Geosyst.*, *7*, Q03002, doi:10.1029/2005GC001094.

Schouten, H., M. A. Tivey, D. J. Fornari, D. Yoerger, A. Bradley, M. Edwards, and P. Johnson (2003), Central anomaly magnetization high: Constraints on the volcanic construction and architecture of young upper oceanic crust, EPR 9–10N, *Ridge2000 Events*, *1*, 30–34.

Shank, T. M., D. J. Fornari, K. Von Damm, M. D. Lilley, R. M. Haymon, and R. A. Lutz (1998), Temporal and spatial patterns of biological community development at nascent deep-sea hydrothermal vents along the East Pacific Rise, *Deep-Sea Res.*, *45*, 465–515, doi:10.1016/S0967-0645(97)00089-1.

Shank, T. M., et al. (2006), Initial biological, chemical, and geological observations after the 2005–6 volcanic eruption on the East Pacific Rise, *Eos Trans. AGU*, *87*(52), Fall Meet. Suppl., Abstract V13C-04.

Soule, S. A., D. J. Fornari, M. R. Perfit, M. A. Tivey, W. I. Ridley, and H. Schouten (2005), Channelized lava flows at the East Pacific Rise crest 9–10°N: The importance of off-axis lava transport in developing the architecture of young oceanic crust, *Geochem. Geophys. Geosyst.*, *6*, Q08005, doi:10.1029/2005GC000912.

Soule, S. A., D. J. Fornari, M. R. Perfit, and K. Rubin (2007), New insights into mid-ocean ridge volcanic processes from the 2005–2006 eruption of the East Pacific Rise, 9°46′N–9°56′N, *Geology*, *35*, 1079–1082, doi:10.1130/G23924A.1.

Tolstoy, M., et al. (2006), A sea-floor spreading event captured by seismometers, *Science*, *314*, 1920–1922, doi:10.1126/science.1133950.

Tolstoy, M., F. Waldhauser, D. Bohnenstiehl, R. T. Weekly, and W.-Y. Kim (2008), Seismic identification of along-axis hydrothermal flow on the East Pacific Rise, *Nature*, *451*, 181–184, doi:10.1038/nature06424.

Von Damm, K. L. (2004), Evolution of the hydrothermal system at East Pacific Rise 9°50′N: Geochemical evidence for changes in the upper oceanic crust, in *Mid-Ocean Ridges: Hydrothermal Interactions Between the Lithosphere and*

Ocean, *Geophys. Monogr. Ser.*, vol. 148, edited by C. R. German, J. Lin, and L. Parson, pp. 285–304, AGU, Washington, D.C.

Von Damm, K. L., and M. D. Lilley (2004), Diffuse flow hydrothermal fluids from 9°50′N East Pacific Rise: Origin, evolution and biogeochemical controls, in *The Subseafloor Biosphere at Mid-Ocean Ridges*, *Geophys. Monogr. Ser.*, vol. 144, edited by W. S. D. Wilcock et al., pp. 245–268, AGU, Washington, D.C.

Whitcomb, L. L., D. R. Yoerger, and H. Singh (1999), Combined Doppler/LBL based navigation of underwater vehicles, paper presented at 11th International Symposium on Unmanned Untethered Submersible Technology, Autom. Undersea Syst. Inst., Durham, N. H.

White, S. M., R. M. Haymon, and S. Carbotte (2006), A new view of ridge segmentation and near axis volcanism at the East Pacific Rise, 8°–12°N, from EM300 multibeam bathymetry, *Geochem. Geophys. Geosyst.*, *7*, Q12O05, doi:10.1029/2006GC001407.